Catalysis Today 147S (2009) S71–S75

Contents lists available at ScienceDirect

Catalysis Today

journal homepage: www.elsevier.com/locate/cattod

Development of aligned carbon nanotubes layers over stainless steel mesh monoliths

V. Martínez-Hansen [a], N. Latorre [a], C. Royo [a], E. Romeo [a], E. García-Bordejé [b], A. Monzón [a,*]

[a] Department of Chemical and Environmental Engineering, Institute of Nanoscience of Aragon (INA), University of Zaragoza, 50009 Zaragoza, Spain
[b] Ins. Carboquímica (C.S.I.C.), C/Miguel Luesma Castán 4, 50015 Zaragoza, Spain

ARTICLE INFO

Article history:
Available online 31 July 2009

Keywords:
Carbon nanotubes
Stainless steel mesh monoliths
Catalytic chemical vapour deposition (CCVD)
Carbon nanofibres (CNFs)

ABSTRACT

We have studied the growth of layers of aligned nanocarbonaceous materials (NCM), in particular carbon nanotubes (CNTs) and carbon nanofibres (CNFs), synthesized via catalytic chemical vapour deposition (CCVD) of ethane over the surface of stainless steel mesh monoliths. The NCM coating properties have been optimized studying the effect of pretreatment of the substrate (acid attack, oxidation and reduction), reaction temperature, and C_2H_6 and H_2 feed concentrations. The experimental results indicate that it is possible to obtain aligned bundles of carbon nanotubes and nanofibres uniformly distributed over all the surface of the mesh. These experiments also allow us to find the kinetics of growth of the aligned bundles of CNTs. The preparation of a catalytic coating with good properties such as good adhesion to substrate, open porosity (mesoporosity) to enhance the diffusion of reactants, uniform thickness of NCM layer, good mechanical strength and control over the microstructure of CNTs ensures good activity and durability of the CNT-based structured catalytic reactor.

1. Introduction

Catalytic gas–liquid reactions are usually carried out in reactors type "slurry" or "trickle bed". Slurry reactors are three-phase catalytic reactors in which catalyst with small particles size (1–200 μm) is suspended by mechanical or gas-induced agitation [1]. The reactants and the products are mixed well in the slurry phase reactor and therefore the concentration gradient through liquid phase in the reactor is minimized [2]. However, in these reactors the exit stream must be filtered to remove the solid particles of small diameter [2,3]. Filtration units are expensive, complicated and cause operational problems rather frequently. Moreover, the agitation of the slurry reactor causes attrition of the catalyst particles, resulting in a loss of active materials and in even more problematic filtration. On the other hand, the suspended particles can also cause erosion of the equipment. A trickle bed reactor is a fixed bed of catalyst pellets where gas and liquid flow over the catalyst pellets. The size of the particles is relatively large (1–10 mm). The main drawback of this system is that it produces internal diffusion problems, due to the large size of the catalyst particles, which is limited because of increasing pressure drop through the reactor. Other disadvantage of trickle bed reactors is the possibility of creating hot spots and dry zones in the catalyst surface [3]. In order to overcome these problems, we propose the use of structured catalytic reactors based on metallic supports such as monoliths [4–9], filters, foams or mesh [10–28]. These reactors combine the advantages of conventional reactors because they have an elevated contact surface, favour the internal diffusion and do not need an additional stage of catalyst separation. Structured reactors are rigid three-dimensional structures with large pores or channels that make fluids flow easily with low pressure drop and showing a large lateral surface which is possible to cover with a thin catalyst layer. They have a high void fraction, from 0.7 to 0.9 vs. 0.4 in trickle bed reactors, so pressure drop is much lower [29]. These supports can be classified in different groups: monoliths, foams, membrane catalysts, systems with cloths or fibres structure and other type of systems, in which catalyst is in the form of conventional particles, but they differ in the particles arrangement in the reactor. The most used supports are monoliths or monolithic structures, which consist of parallel longitudinal channels with low cross-section separated by thin walls, over which catalyst is deposited. As well as the form, the channels geometry in monolith can change. To achieve the desired properties, a layer of aligned carbon nanotubes must be created over the surface of the monolith by an "in situ" growth (immobilization) process which serves as reactor catalyst support [30,31]. This new type of structured catalytic reactors could be applied for example in decontamination processes, in both gas and liquid phases, e.g. depuration of water, hydrogen production,

* Corresponding author. Tel.: +34 976761157; fax: +34 976762142.
E-mail address: amonzon@unizar.es (A. Monzón).

0920-5861/$ – see front matter © 2009 Elsevier B.V. All rights reserved.
doi:10.1016/j.cattod.2009.07.010

e.g. by NH_3 decomposition, or intensification of chemical processes by increasing selectivity and reducing by-product generation. The main goal of this paper is the optimization of the growth process of aligned carbon nanotubes over the external surface of structured metallic supports. One of very recent areas of interest in the production of CNTs is the large-scale synthesis of vertically aligned carbon nanotubes (VA-CNT) [32,33]. One of the most promising methods is the CCVD of hydrocarbons in presence of oxygen [32,33]. We have studied the kinetics of NCM growth over stainless steel mesh monoliths, and the influence of the activating (mesh pretreatment, oxidation temperature and reduction temperature), and operating (reaction temperature and feed composition) conditions over the type and morphology of the carbonaceous layer formed by catalytic chemical decomposition (CCVD) of ethane. The stainless steel substrate has been characterized before and after reaction with the aim of examining the changes in its structure, and also the type and properties of the deposited carbonaceous layer.

2. Experimental

The monoliths used as catalyst and support for the reaction CCVD of ethane have been made of stainless steel mesh (AISI 316L, Filtra®, hole = 100 μm, diameter wire = 63 μm).

The mesh was cut into pieces of 42 mm × 20 mm and rolled up forming single or multiwall monoliths. This option easily allows building monoliths with different ratios of external surface area/monolith volume. The experiments were carried out at atmospheric pressure in a thermobalance (CI Electronics Ltd., UK, model MK2) operated as a differential CCVD reactor. This experimental system allows continuous recording of the sample weight and temperature during all the steps of an experiment. Previous to the reaction, the monolith was treated with acid to clean the surface. The metallic monolith, with the desired ratio area/volume, is placed on the thermobalance basket and then is oxidized and reduced in situ. After the activation steps, the CCVD reaction with $C_2H_6/H_2/N_2$ mixtures produces the growth of a layer of nanocarbonaceous material over the external surface of the monolith. From this type of experiments we can calculate not only the NCM growth rate, but also the kinetics of reduction and reaction stages. In addition, from the values of the difference between the weights after oxidation and reduction steps; and the bulk mesh composition can be used to estimate the amount of reduced metal. A typical composition of the stainless steel mesh 316L is shown in Table 1. This composition indicates that after the reduction stage, the active sites for CCVD reaction will be the nanoparticles of Fe and Ni (or Fe–Ni alloys) segregated to the external surface of the wires after the activation stages. The operating conditions studied are presented in Table 2. After reaction, the monolith, as well as the carbon obtained, was characterized by scanning electronic microscopy and RAMAN spectroscopy. SEM images were obtained using a JEOL JSM 6400 instrument. A Horiba Jobin Yvon HR800 UV model equipped with a CCD (charge coupled device) was used to get the RAMAN spectra.

Table 1
Typical bulk composition of stainless steel 316L.

% Fe[a]	% Cr	% Cr	% Ni	% C	% Mn	% Si	% P	% S	% N	Mo
43–54	16–18	16–18	10–14	0.08	2	0.75	0.045	0.03	0.10	2.0–3.0

[a] Balance.

Table 2
Range of experimental conditions during CCVD of ethane.

Stage	Temperature (°C)	Time (min)	Flow (N ml/min)
Oxidation	From 700 to 900	60	100 air/100 N_2
Reduction	From 700 to 900	60	100 H_2/100 N_2
Reaction	From 700 to 900	30	H_2: from 0 to 200, C_2H_6: from 25 to 200, N_2: until 600

3. Results and discussion

3.1. Influence of the activation stages: acid pretreatment, oxidation and reduction

Before the CCVD reaction studies, it has been investigated the effect of the acid pretreatment, of the activation and reduction steps and, the effect of the elimination of some of these steps, on the rate of growth of the carbonaceous layer. Figs. 1 and 2 collect the SEM results of these studies. The mesh of the monolith was utilized fresh (as received), or after an acid treatment with HCl (37%) at room temperature during 30 min. In both cases the operating conditions were: oxidation temp.: 800 °C; reduction temp.: 700 °C; reaction temp.: 800 °C, total flowrate: 600 N ml/min, feed composition ($\%H_2/\%C_2H_6/\%N_2$): 1.67/16.67/81.67. The use of the acid pretreatment increases the surface roughness and cleans the surface of the mesh [28]. In consequence, a beneficial effect over time evolution of the mass of carbon layer (C_C) is observed. The quantity of carbonaceous material obtained augments twice, from 1.8% of carbon from 3.7%, after acid treatment. In addition, as can be seen from SEM results (Fig. 1a and b) the beneficial effect of acid pretreatment it is not only the increase of mass of carbon growth, but more interestingly, the distribution of the layer of carbonaceous material formed is much more homogeneous after the acid pretreatment. Therefore, an acid pretreatment of the metallic surface it is necessary to obtain large quantities of continuous and homogenous layer of carbonaceous deposits.

As regards, the effect of the oxidation and reduction steps, we have investigated not only the effect of the level of temperatures used in each stage, but also the effect of the elimination of some of these activation stages.

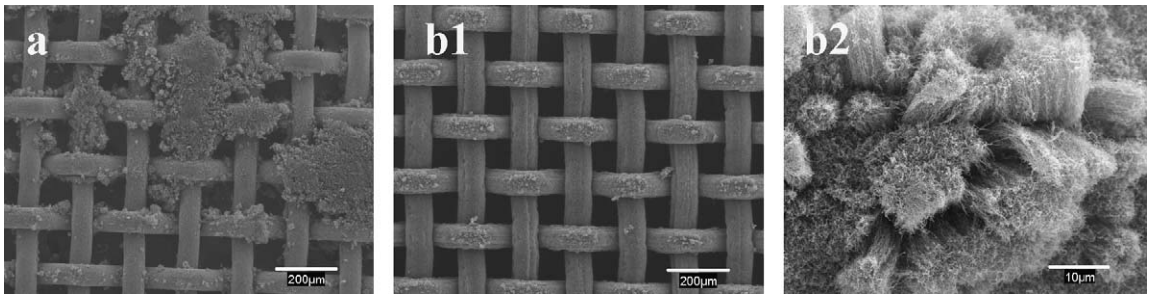

Fig. 1. SEM images of the mesh (a) after oxidation, reduction and reaction (b1 and 2) after HCl treatment, oxidation, reduction and reaction.

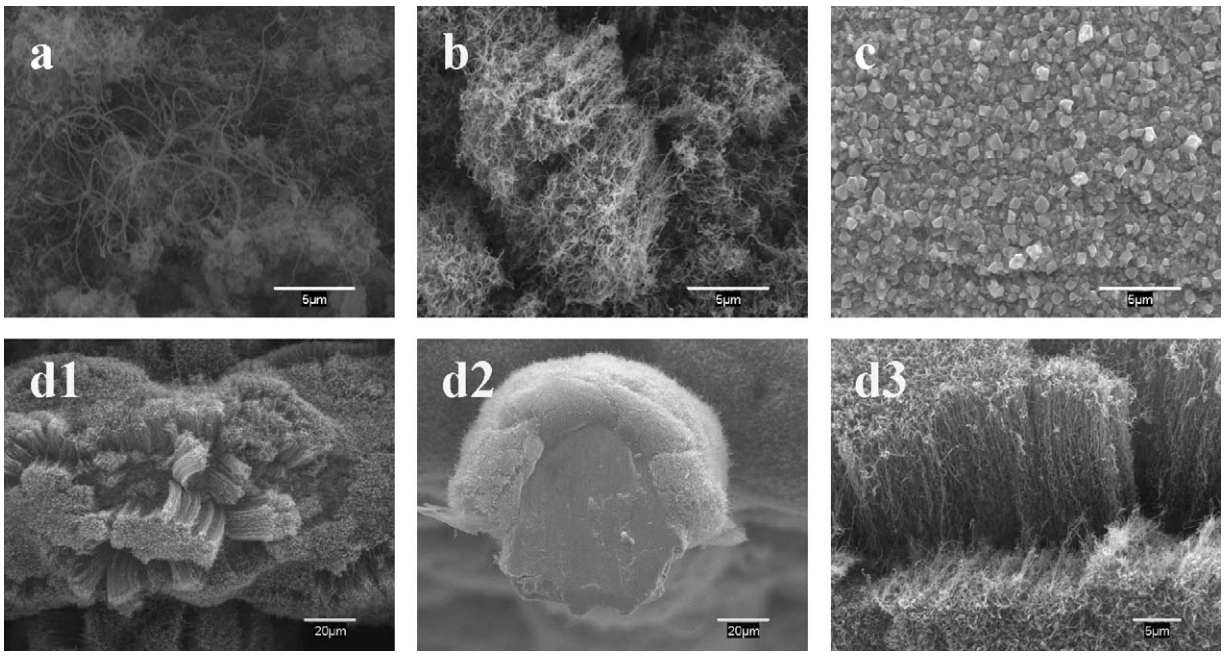

Fig. 2. SEM images of the mesh after reaction at different temperatures of oxidation (a) 700 °C, (b) 800 °C, (c) 900 °C, (d1–3) after oxidation, reduction and CCVD reaction at 800 °C.

The oxidation process modifies the external surface of the wires, creating cracks and break-ups, and, in consequence, increasing the surface area [22]. After the reduction step, the external nanoparticles of iron oxide are converted to active metallic sites for the CCVD reaction [22,34]. Thus, several experiments were carried out to study the carbon growth after direct reaction (i.e. without oxidation and reduction steps), after oxidation and reaction (i.e. without reduction step), after reduction and reaction (i.e. without oxidation step), and finally performing all the steps. The operating conditions were: oxidation temp.: 800 °C; reduction temp.: 700 °C; reaction temp.: 800 °C, total flowrate: 600 N ml/min, feed composition (%H_2/%C_2H_6/%N_2): 1.67/16.67/81.67. The highest yield (3.8%) is obtained when all the stages (oxidation and reduction) are carried out consecutively. Obviously, the elimination of the oxidation step has little effect with respect to the case without oxidation and reduction steps (2.9 and 3.0%, respectively). The elimination of reduction step is less important from the point of view of carbon yield (3.3%) because the necessary reduction of metallic oxides, mainly Fe, is produced directly during the CCVD reaction by the hydrocarbon/hydrogen mixture. However, RAMAN results (see Table 3) indicate that the quality of the carbonaceous layer is lower in this case, as is showed by the higher values of I_D/I_G ratios. In this case, the incomplete reduction of oxide nanoparticles can difficult the selective CNT growth, favouring the formation of amorphous carbon on the surface of the nanoparticles [22]. After the decomposition of the hydrocarbon molecules, the mechanism of CNT formation considers the development of a layer of unstable carbide at the surface of the reduced metallic particles [35,36]. The decomposition of this carbide leaves carbon atoms inside the metallic particles that can diffuse through them and then precipitate nucleating the nanotubes. This process can obviously obstructed if the reduction of the metallic particles is incomplete, and "islands" of metallic oxide are present at the surface. If the diffusion process is hindered, the carbon atoms leaved at the metallic surface after the hydrocarbon decomposition can form encapsulating carbon layers, which deactivate the catalytic particles [37–39].

This result is a considerable decrease of the quality of the NCM formed. In Fig. 1b is shown the large quantity of bundles of aligned carbon nanotubes produced when all the steps are carried out. Consequently, the external surface of the mesh has been changed and prepared for the selective production of a homogeneous layer of CNTs. If the oxidation or the reduction steps are eliminated before the reaction, the quantity and quality of the nanocarbonaceous layer is clearly decreased. As regards, the effect of the level of the oxidation temperature used, the best conditions are found at 800 °C, obtaining a good yield (3.7%), and a good quality of the produced layer of carbonaceous material as indicate SEM (Fig. 2b) and RAMAN results (Table 3). SEM images show the formation of a homogeneous layer of CNTs and CNFs over all the wires of the mesh. When the oxidation temperature is lower, the carbon content is also high but a large quantity of amorphous carbon appears (Fig. 2a) increasing the value of I_D/I_G ratio (Table 3). At 900 °C the metallic monolith is almost inactive due to the strong crystallization of the metallic surface (Fig. 2c). Probably this strong crystallization degree has inhibited the effective reduction of the nanoparticles of metallic oxide hindering the growth of carbon nanotubes. The reduction temperature was also changed to try to increase the carbon yield and/or improve its quality. The results indicate that the metallic mesh presents good carbon productivity in the entire range of reduction temperatures studied (700–900 °C). An increase in the reduction temperature results in an augment in the number of active metallic sites, which enhances the carbon yield (3–4%). Large quantities of bundles of CNTs are observed in all the cases. However, the monolith becomes fragile after the use at 900 °C, which difficulties its use in an industrial process. Furthermore, the use of the same temperature in all the stages of the experiment can make easier the integration of the process for an industrial use, decreasing the thermal fatigue. In consequence, the optimum reduction temperature could be considered 800 °C. Results in Table 3 indicate that under these operating condition is obtained a good carbon yield, 3.3%, maintaining at the same time good quality of the NCM formed, I_D/I_G = 0.589. In Fig. 2d it is possible to observe the profile of one the wires of the mesh, distinguishing the core of a wire from the bundles of carbon nanotubes. The average final length of the bundles is about 20 μm.

Table 3
Experimental results.

Oxidation temp. (°C)	Reduction temp. (°C)	Reaction			CC final (%)	$r_{C,max} \times 10^3$ (g/g monolith min.)	I_D/I_G [a]
		Temp. (°C)	% H_2	% C_2H_6			
800[b]	700	800	1.67	16.67	1.8	1.84	0.916
800	700	800	1.67	16.67	3.7	4.64	0.589
–	–	800	1.67	16.67	2.9	3.90	0.705
–	700	800	1.67	16.67	3.0	2.97	0.577
800	–	800	1.67	16.67	3.3	3.50	0.726
700	700	800	1.67	16.67	3.7	4.61	0.801
900	700	800	1.67	16.67	0.3	0.14	0.954
800	800	800	1.67	16.67	3.3	4.09	0.589
800	900	800	1.67	16.67	4.0	4.50	0.554
800	800	700	1.67	16.67	0.3	0.30	–
800	800	900	1.67	16.67	4.3	9.02	0.930
800	800	800	0	16.67	2.1	2.33	–
800	800	800	16.67	16.67	3.1	2.82	–
800	800	800	33.33	16.67	2.2	2.35	–
800	800	800	1.67	4.16	1.4	1.07	–
800	800	800	1.67	8.33	2.2	1.70	–

[a] Determined from Raman spectra (not shown).
[b] Experiment without HCl pre-treatment.

3.2. Influence of CCVD operating conditions: temperature and feed composition

The main operational variables are the CCVD reaction temperature and the gas feed composition. The effect of the reaction temperature on the carbon content is shown in Fig. 3a. It can be observed that carbon content augments when reaction temperature increases. An augment in the operating temperature produces the increment of the rate of ethane decomposition over the surface of the iron nanoparticles created after the reduction step. However, the kinetic behaviour is very different at three temperatures studied. At 700 °C the sample present low activity and the carbon yield obtained is very low (0.3%). At 800 °C the sample is quite active, but more important, it is very selective to the desired nanocarbonaceous material, obtaining homogeneous layers containing bundles of aligned CNTs (see for example SEM images in Figs. 1b, 2b and d). In addition, TEM result indicates that the CNTs formed are MWNT (not shown). However, the reaction rate at this temperature decreases along operation time, probably as a consequence of the deactivation of the metallic nanoparticles [37–39]. Finally, at 900 °C, the amount of carbon produced is the highest but it is quite more heterogeneous. The carbonaceous material obtained is much less ordered appearing wide and short fibres without any alignment. Therefore, the selected as optimum reaction temperature is 800 °C. As regards, the effect of the gas feed composition (Fig. 3b and c), shows the evolution of carbon yield along time for different partial pressures of hydrogen (Fig. 3b) and ethane (Fig. 3c). All the experiments were carried out at 800 °C, and the total flowrate was 600 N ml/min.

The concentration of hydrogen was varied from 0 to 33.3%. The presence of a small amount of hydrogen in the feed (1.67%) provokes a great increase in the carbon yield, increasing mainly the initial rate of CNT formation. However, as the hydrogen concentration increases, the carbon yield decreases from this maximum, attaining, at 33.3% of hydrogen, the same carbon yield that in the case of 0% of hydrogen in the feed. The presence of this maximum in the carbon yield as a function of the hydrogen concentration is explained because at low concentrations, hydrogen prevents the formation of encapsulating carbon, avoiding catalyst deactivation [37–40]. However, at high hydrogen concentrations the competition between H_2 and C_2H_6 for the metallic surface sites causes a diminution in the net rate of CNT formation [39,40]. Therefore, as the hydrogen concentration increases, the amount of carbon formed decreases. However, the addition of hydrogen in the feed seems not to affect significantly to the carbon morphology of the samples after reaction (results not shown). Finally, concerning to the effect of feed ethane concentration, results in Fig. 3c show that, an increase in ethane partial pressure boost both the amount of produced carbon, but also the deactivation rate. In addition, at low partial pressures of ethane,

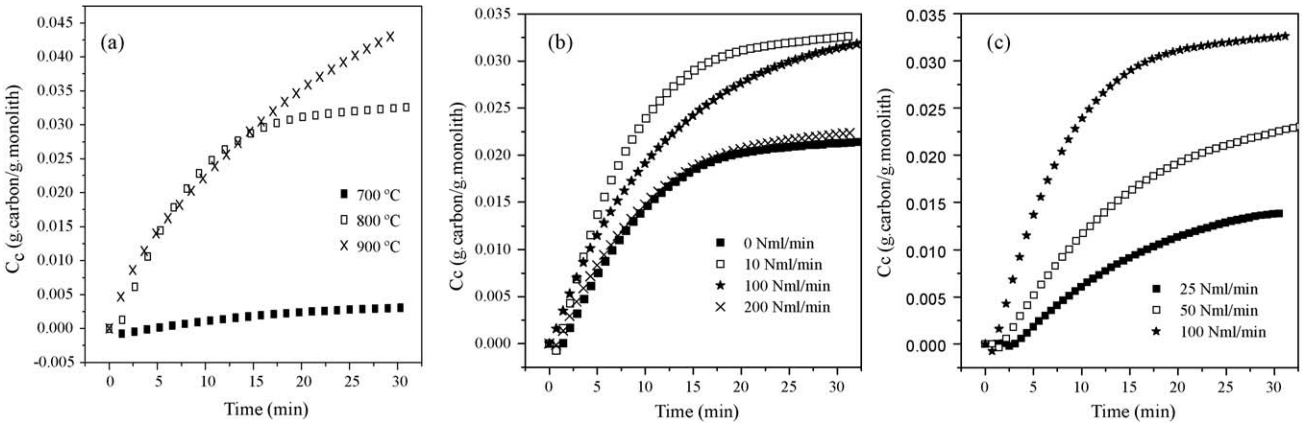

Fig. 3. Influence of operating conditions on the evolution of carbon content. (a) Reaction temperature, (b) partial pressure of hydrogen (0%, 1.7%, 16.7% and 33.3% of H_2, respectively) and (c) partial pressure of ethane (4.2%, 8.3% and 16.7% of C_6H_6, respectively).

the initial period of induction of the CNT formation is higher due to the low rate of carburization of the metallic nanoparticles [39]. Higher ethane concentrations enhance the diffusion–precipitation process through the metallic crystallites, increasing the initial reaction rate [36]. However, the greater the concentration of ethane, the greater is the rate of formation of carbon species which encapsulate and deactivate the surface of the metallic crystallites [37–39].

4. Conclusions

The CCVD of ethane over metallic stainless steel mesh is a good method to produce homogeneous layers of aligned bundles of CNTs. The surface of raw stainless steel mesh was modified via acid attack with HCl (37%), ensuring a uniform distribution of the carbonaceous layer. On the other hand, an adequated selection of the activation (oxidation and reduction) temperatures improves both the carbon yield and the uniform distribution of the CNTs layer. The experimental sequence that provides the best results is: oxidation, reduction and reaction. Oxidation leads to the formation of superficial cracks, break-ups and crevice. Reduction leads to the formation of the segregated metallic nanoparticles at the external surface of the wires. These nanoparticles are the active sites for the CCVD reaction. Both activation stages modify and prepare the mesh surface for the reaction. The optimum temperature obtained for these processes was 800 °C. The mesh used in the study needs operating temperatures higher than 700 °C to be active. Over 900 °C the material is very active, but becomes fragile. If all the stages are carried out at the same temperature, 800 °C, a uniform layer of NMC is obtained over the surface of the mesh, forming a large quantity of bundles of aligned CNTs, mainly MWNT. The presence of little amounts of hydrogen in the feed favours the activity and the stability of the monolith during the carbon layer formation. This is due to the regenerating effect of hydrogen, which inhibits encapsulating carbon deposition that deactivates the metallic particles. But, upper hydrogen concentration decrease the net rate of CNTs formation due to competitive effect with the ethane for the metallic active sites. An increase in the ethane concentration enhances both the carbon formation and the deactivation rates. The increase in ethane concentration boosts the driving force for the CNTs formation, increasing the number of CNTs that can be formed, and their nucleation rate.

Acknowledgment

The authors acknowledge financial support from MICINN (Spain)-FEDER, Project CTQ 2007-62545/PPQ.

References

[1] Y.T. Shah, Recent advances in trickle bed reactor, in: Concept & Design of Chemical Reactors, Gordon and Breach Sci. Pub., New York, 1986, p. 299.
[2] A. Cybulski, J.A. Moulijn, Structured Catalysts and Reactors, Marcel Dekker, New York, 1998.
[3] J.F. Jenck, Heterogeneous catalysis and fine chemicals II, Stud. Surf. Sci. Catal. 59 (1991) 1.
[4] M.T. Kreutzr, P. Du, J.J. Heiszwolf, F. Kapteijn, J.A. Moulijn, Chem. Eng. Sci. 56 (2001) 6015.
[5] T.A. Nijhuis, M.T. Kreutzer, A.C. Romijn, F. Kapteijn, J.A. Moulijn, Chem. Eng. Sci. 56 (2001) 823.
[6] T.A. Nijhuis, M.T. Kreutzer, A.C. Romijn, F. Kapteijn, J.A. Moulijn, Catal. Today 66 (2001) 157.
[7] F. Kapteijn, T.A. Nijhuis, J.J. Heiszwolf, J.A. Moulijn, Catal. Today 66 (2001) 133.
[8] A.E. Beers, R.A. Spruijt, T.A. Nijhuis, F. Kapteijn, J.A. Moulijn, Catal. Today 66 (2001) 175.
[9] G. Kolb, V. Hessel, Chem. Eng. J. 98 (2004) 1.
[10] L. Kiwi-Minsker, I. Yuranov, V. Holler, A. Renken, Chem. Eng. Sci. 54 (1999) 4785.
[11] L. Kiwi-Minsker, I. Yuranov, V. Holler, A. Renken, Catal. Today 69 (2001) 175.
[12] Y. Matatov-Meytal, V. Barelko, I. Yuranov, M. Sheintuch, Appl. Catal. B 27 (2000) 127.
[13] Y. Matatov-Meytal, V. Barelko, I. Yuranov, L. Kiwi-Minsker, A. Renken, M. Sheintuch, Appl. Catal. B 27 (2000) 233.
[14] Theo Vergunst, Carbon coated monolithic catalysts, PhD Thesis, 1999, Delft.
[15] F. Kapteijn, J.J. Heiszwolf, T.A. Nijhuis, J.A. Moulijn, CATTECH 3 (1) (1999) 24.
[16] Y. Matatov-Meytal, M. Sheintuch, Appl. Catal. A 231 (2002) 1.
[17] M.F. Zwinkles, S.C. Jaras, P.G. Menon, T.A. Grifin, Catal. Rev. Sci. Eng. 35 (1993) 317.
[18] W.F. Maier, J.W. Schlangen, Catal. Today 17 (1993) 225.
[19] M. Valentini, G. Groppi, C. Cristiani, M. Levi, E. Tronconi, P. Forzatti, Catal. Today 69 (2001) 307.
[20] R.E. Hayes, S.T. Kolaczkowski, P.K. Li, S. Awdry, Chem. Eng. Sci. 56 (2001) 4815.
[21] S. Siemund, J.P. Leclerd, D. Schweich, M. Prigent, F. Castagana, Chem. Eng. Sci. 51 (1996) 3709.
[22] R.L. Vander Wal, L.J. Hall, Carbon 41 (2003) 659.
[23] N.A. Jarrah, F.H. Li, J.G. van Ommen, L. Lefferts, J. Mater. Chem. 15 (2005) 1946.
[24] N.A. Jarrah, J.G. van Ommen, L. Lefferts, J. Mater. Chem. 14 (2004) 1590.
[25] N.A. Jarrah, J.G. van Ommen, L. Lefferts, Catal. Today 79 (2003) 29.
[26] N.A. Jarrah, J.G. van Ommen, L. Lefferts, J. Catal. 239 (2006) 460.
[27] P. Tribolet, L. Kiwi-Minsker, Catal. Today 102 (2006) 15.
[28] V. Meille, Appl. Catal. A 315 (2005) 1.
[29] Yu. Matatov-Meytal, M. Sheintuch, Appl. Catal. A 231 (2002) 1.
[30] P. Serp, M. Corrias, P. Kalck, Appl. Catal. A-Gen. 253 (2003) 337.
[31] M.A. Ulla, A. Valera, T. Ubieto, N. Latorre, E. Romeo, V.G. Milt, A. Monzón, Catal. Today 133–135 (2008) 7.
[32] K. Hata, D.N. Futaba, K. Mizuno, T. Namai, M. Yumura, S. Iijima, Science 306 (2004) 1362.
[33] E. Einarsson, Y. Murakami, M. Kadowaki, S. Maruyama, Carbon 46 (2008) 923.
[34] R. Philippe, B. Caussat, A. Falqui, Y. Kihne, P. Kalck, S. Bordère, D. Plee, P. Gaillard, D. Bernardg, P. Serp, J. Catal. 263 (2009) 345.
[35] I. Alstrup, J. Catal. 109 (1988) 241.
[36] J.-W. Snoeck, G.F. Froment, M. Fowles, J. Catal. 169 (1997) 240.
[37] K.P. de Jong, J.W. Geus, Catal. Rev. -Sci. Eng. 42 (2000) 481.
[38] M.L. Toebes, J.H. Bitter, A. Jos van Dillen, K.P. de Jong, Catal. Today 76 (2002) 33.
[39] J.I. Villacampa, C. Royo, E. Romeo, J.A. Montoya, P. Del Angel, A. Monzón, Appl. Catal. A: Gen. 252 (2003) 363.
[40] Y. Li, J. Chen, L. Chang, Y. Qin, J. Catal. 178 (1998) 76.